Superior Mass Transfer Properties of Technical Zeolite Bodies with Hierarchical Porosity

*Laurent Gueudré, Maria Milina, Sharon Mitchell, and Javier Pérez-Ramírez**

Mass transfer in zeolite crystals can be enhanced by the introduction of a hierarchical network of auxiliary mesopores. To fully exploit pore engineering in the design of more efficient industrial catalysts, the benefit needs to be demonstrated over technically relevant forms. Here, the influence of shaping on the adsorption and diffusion properties of hierarchical ZSM-5 is assessed by studying the gravimetric uptake of 2,2-dimethylbutane over powders and millimeter-sized bodies. Formed by extrusion or granulation with clay binders, the latter display a complex trimodal network of micro-, meso-, and macropores. The enhanced intracrystalline diffusivity due to the interconnected mesopores is preserved in the macroscopic bodies, independent of the shaping method or binder applied. Furthermore the superior overall diffusivity is retained in the hierarchical bodies compared to their conventional (purely microporous) counterparts, despite the significant extracrystalline resistance to mass transfer. The connective participation of mesopores, leading to a 6 times improved effective diffusivity in hierarchical with respect to conventional zeolite powders, is revealed by the distinct dependence on the adsorbate concentration and the relationship with the mesopore surface area. Analysis of the thermodynamic parameters derived from the adsorption isotherm proves a sensitive method to detect binder-zeolite interactions induced upon shaping.

1. Introduction

Mass transfer is an omnipresent phenomenon in nature and technology determining, in many cases, the performance of the ongoing processes. Consideration of diffusion properties is particularly important for application of porous materials as catalysts, sorbents, and ion exchangers.[1–3] Zeolites, featuring micropores of molecular dimensions, are a prime example of a material whose productivity is hampered by hindered transport to and from internal active sites. In the last decades, two different approaches have been developed to alleviate the diffusion limitations imposed by the zeolitic structure, including the syntheses of wide-pore and hierarchically organized zeolites.[4–8] The latter type of materials combines the intrinsic microporosity with an auxiliary network of interconnected meso- and/or macropores and can be prepared by direct or post-synthetic strategies.[8–11] Silicon leaching by alkaline treatment is an effective, versatile, and scalable top-down method for the introduction of intracrystalline mesoporosity in zeolites.[12] The resulting hierarchical zeolites exhibit superior catalytic performance compared to conventional zeolites in a wide range of gas- and liquid-phase reactions.[7,13] This enhancement is commonly attributed to facilitated molecular diffusion within the zeolite crystals, yet only limited studies[14–25] have assessed the relative mass transfer properties of hierarchical with respect to conventional (exhibiting micropores only) zeolites (**Table 1**). Two interrelated ideas have been put forward to explain the contribution of the secondary pore network. The first considers only the decrease in the mean diffusion path in the micropores,[13,16,18] while the second, in addition, proposes that the larger pores directly contribute to the kinetics and thermodynamics of the diffusion process.[21,26–28]

Until now, most studies dealing with mass transfer in hierarchical zeolites have been performed on materials that are not representative of industrially relevant samples. These investigations are limited to the characterization of pure zeolite powders, often consisting of larger crystals. Therefore, it is required for potential large-scale catalytic applications to assess whether technical zeolites, consisting of relatively small crystals compacted with the aid of binders into millimeter-sized bodies can preserve the adsorption properties reported for powdered samples. Recent works by our group tackled the manufacture and in-depth characterization of granules and extrudates of desilicated ZSM-5 zeolite.[29–31] In technical form, the hierarchical zeolites exhibited superior lifetime and selectivity in the conversion of methanol to olefins.[31] Despite the fact the improved performance was attributed to enhanced transport properties, the latter were not explicitly assessed. As shown in **Figure 1**, the porosity of the hierarchical shaped bodies consists of micropores intrinsic to the MFI framework (pore diameter 0.56 nm), mesopores centered around 10 nm introduced into the zeolite crystals through alkaline leaching, and macropores centered around 250 nm which are defined upon agglomeration

Dr. L. Gueudré, M. Milina, Dr. S. Mitchell,
Prof. J. Pérez-Ramírez
Institute for Chemical and Bioengineering
Department of Chemistry and Applied Biosciences
ETH Zurich
Wolfgang-Pauli-Strasse 10
CH 8093, Zurich, Switzerland
E-mail: jpr@chem.ethz.ch

DOI: 10.1002/adfm.201203557

Table 1. Overview of relevant diffusion studies involving hierarchical zeolite powders.

Zeolite	Synthesis method	Technique[a)]	Crystal size [μm]	Probe molecule	Improvement[b)]	Ref.
ZSM-5	Solid-phase crystallization	ZLC	0.3; 90	*n*-heptane; toluene	10^5	[22]
	Desilication	TEOM	3 × 5 × 17	neopentane	10^2	[14]
	Carbon templating	Elution	1	*i*-butane	3	[17]
	Desilication	Gravimetry	–	cumene	10^2–10^3	[15]
	Desilication	IR	0.25; 17 × 4 × 4	*o*-xylene	4	[18]
	Desilication followed by acid washing	IR	–	benzene	2.4	[16]
A	Supramolecular templating	PFG NMR	2	water	n.q.[c)]	[23]
	Supramolecular templating	PFG NMR	2	propane	10^2–10^3	[19,20]
Beta	Supramolecular templating	PFG NMR	0.2–1	water	3	[23]
Y	Steaming	PFG NMR	3	*n*-octane; 1,3,5-triisopropylbenzene	unaffected	[21]
Ferrierite	Desilication	Elution	0.3 – 0.8 × 0.05–0.15	*n*-butane; *i*-butane	n.q.	[25]
ITQ-4	Desilication	Elution	1.5 × 0.2 × 0.2	*n*-butane; neopentane	n.q.	[24]

[a)]PFG NMR: pulsed field gradient nuclear magnetic resonance; ZLC: zero length column; TEOM: tapered element oscillating microbalance; IR: infrared spectroscopy; [b)]Extent of the improvement in mass transfer with respect to the conventional zeolite; [c)]n.q.: not quantified.

of the zeolite and binder particles. Although the intracrystalline mesoporosity seems to be preserved in the technical bodies, the zeolite-binder interaction and the imposed macroporosity could change the mass transfer picture. The possibility to retain equivalent kinetic and thermodynamic properties of adsorption upon shaping hierarchical zeolites remains unexplored.

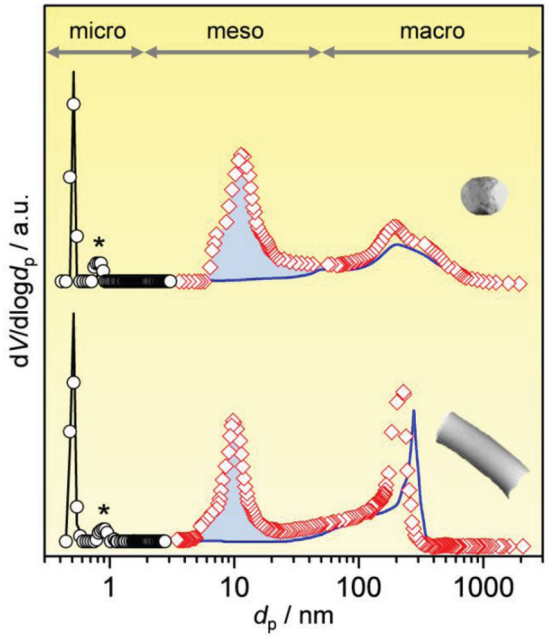

Figure 1. Trimodal pore size distribution in the hierarchical ZSM-5 a) granules and b) extrudates, determined from argon adsorption (circles) and mercury porosimetry (diamonds). The lines represent the bimodal pore network of the conventional zeolite bodies. The peak with the asterisk is an artifact associated with a phase transition of Ar. Adapted with permission.[31] Copyright 2012, Nature Publishing Group.

Herein, we perform a systematic gravimetric study on the diffusion of the branched alkane, 2,2-dimethylbutane (2,2DMB, kinetic diameter of 0.61 nm), in desilicated ZSM-5 powders and shaped bodies. As a first step to determine the impact of shaping on the adsorption properties, we quantify the mass transfer improvement over the hierarchical with respect to conventional zeolite powders. The origin of this effect is demonstrated by determining the diffusion mechanism imposed by the auxiliary pore network. Thereafter, we assess the effect of granulation and extrusion in the presence of attapulgite and kaolin clay binders on the mass transfer properties of conventional and hierarchical zeolites by using a model taking into account the different levels of porosity in the technical bodies.

2. Methodology

This section outlines the approach followed to determine whether the diffusion properties of hierarchical zeolites are preserved upon shaping. For that purpose, a detailed analysis of the adsorption properties of the conventional and hierarchical zeolites powders and technical forms is required. A gravimetric technique was chosen as a versatile method to characterize the samples.

2.1. Diffusion in Powders

In an isothermal system and in the absence of thermal and particle bed effects (Supporting Information Figure SI1), the sorption kinetics are governed by the intracrystalline diffusion process. Therefore, the transient uptake curves observed over powders can be described by Equation 1,[1,32] assuming spherical crystals of radius r_c:

$$\frac{q_t}{q_\infty} = 1 - \frac{6}{\pi^2}\sum_{n=1}^{\infty}\frac{1}{n^2}\exp\left(\frac{-n^2\pi^2 D_c t}{r_c^2}\right) \quad (1)$$

where D_c is the effective diffusion coefficient. While a model taking the crystal size dispersion into account could be considered more appropriate,[33] no analytical solution exists to describe an adsorbent with intra- and extracrystalline porosity and a dispersed crystal size. Since these factors are relevant in order to study mass transfer in zeolite granules and extrudates (vide infra), the validity of the classical model was first evaluated in comparison with a more parameterized approach. As shown in Supporting Information Figure SI2, the good agreement in fit and correspondingly in D_c, proved that consideration of the crystal size dispersion was of relatively minor importance to describe the gravimetric results of this study. Indeed, for samples of heterogeneous crystal size a much larger error can be expected if only the short or long time regions of the uptake curve are considered than that obtained by fitting the entire curve. Additionally, it should be mentioned that the effect of the crystal size dispersion is less pronounced within the shaped zeolites due to the effect of the macropore resistance in the agglomerated body (vide infra).

2.2. Diffusion in Technical Bodies

In order to interpret the kinetic data derived for the shaped zeolite bodies, which comprise multiple interconnected pore networks, two distinct diffusion processes are considered: i) extracrystalline in the macropores of the consolidated granules or extrudates and ii) intracrystalline within the zeolite crystals. Because the intra- and extracrystalline diffusivities cannot be independently measured by conventional techniques, a model consisting of Equations 2–5 is used to describe the experimental uptake curves:[34]

$$\frac{q_t}{q_\infty} = 1 - \sum_{m=1}^{\infty}\sum_{n=1}^{\infty}\frac{36n^2\pi^2\exp\left(\frac{-p_{n,m}^2 D_c t}{r_c^2}\right)}{\beta^2 p_{n,m}^4\left(1+\frac{\cot an\, p_{n,m}}{p_{n,m}}(p_{n,m}\cot an\, p_{n,m}-1)\right)} \quad (2)$$

where $p_{n,m}$ is given by:

$$\beta(p_{n,m}\cot an\, p_{n,m} - 1) = -n^2\pi^2 \quad (3)$$

$$\beta \equiv \frac{3\alpha(1-\varepsilon_p)q_0}{\varepsilon_p c_0} \quad (4)$$

where the sorbate concentration (q_0) is in equilibrium with the fluid concentration (c_0).

$$\alpha \equiv \frac{D_c}{r_c^2}\frac{R_p^2}{D_p} \quad (5)$$

In this formula, D_p is the diffusion within the macropores and R_p the particle (granule or extrudate) radius.

Assuming that the intracrystalline diffusivity is not affected by the shaping process and that the difference between the experimental and theoretical diffusivities within the macropores originates from the tortuosity (τ), it is possible to derive an expression for D_p:

$$D_p = \frac{D_K}{\tau} \quad (6)$$

where D_K is the Knudsen diffusivity:

$$D_K = 97 r_p\sqrt{\frac{T}{M}} \quad (7)$$

In this equation, r_p is the macropore radius and M the molecular weight of the probe molecule.

The correspondence between the theoretical and experimental extracrystalline diffusivities obtained for the conventional and hierarchical zeolites in shaped form, and hence the relative tortuosity of these two materials, is a suitable tool to evaluate the influence of shaping on the intracrystalline diffusivity. While the slightly different macroporosities evidenced in the shaped bodies (Figure 1) influence the Knudsen diffusivity of the conventional and hierarchical materials, this variation does not strongly impact the estimated average tortuosity.

To gauge the relative contribution of the intra- and extracrystalline pore networks to the overall mass transfer, characteristic diffusion time constants are estimated for each porosity level:

$$t_{intra} = \frac{r_c^2}{D_c} \quad (8)$$

$$t_{extra} = \frac{R_p^2}{D_e} \quad (9)$$

where D_c is the effective diffusivity in the micropores assessed for powder samples and D_e the effective diffusivity in the macropores, which depends on the Henry's constant (K) according to:

$$D_e = \frac{D_p\varepsilon_p}{\varepsilon_p + (1-\varepsilon_p)K} \quad (10)$$

$$K = K_0\exp\left(-\frac{\Delta U}{RT}\right) \quad (11)$$

where K_0 represents the pre-exponential factor and ΔU the internal energy of adsorption.

The characteristic diffusion time represents the time for a guest molecule to penetrate to the center of a zeolite crystal (t_{intra}) or a shaped body (t_{extra}), while the total diffusion time is obtained by addition of the individual contributions. A global diffusion time (t_{global}) is also considered. Since the latter is derived by fitting the normalized uptake curves with Equation 1, the total and global diffusion times should be identical if the intra- and extracrystalline resistances are precisely estimated. A major advantage of estimating the diffusion times is that it permits the direct calculation of an average particle tortuosity. The latter parameter enables complete correlation of the theoretical values (t_{intra}, t_{extra}, and t_{total}) with the experimental data (t_{global}) obtained at different temperatures. This provides a more accurate estimation of tortuosity, than determined by fitting the

data obtained at each temperature independently. The agreement between t_{global} and t_{total} diffusion times, observed on comparison of the experimental and calculated contributions of t_{intra} and t_{extra} to the overall mass transfer, validate the determined diffusivity.

3. Results and Discussion

The results and discussion are divided into two main parts. In the first, the mass transfer improvement is quantified in hierarchical zeolite powder (HP) in comparison with the conventional sample (CP). The origins of the enhanced diffusion are assessed by studying the thermodynamic and kinetic properties of adsorption of 2,2DMB at different concentrations and with hierarchical zeolites of varying mesopore surface area. In the second part, the effect of the shaping process on the mass transfer properties is assessed using granules and extrudates derived from the conventional and hierarchical zeolites with the respective addition of attapulgite and kaolin binders. A complete summary of the set of samples studied, including the preparation conditions and the porous properties, is available in the supplementary information (Supporting Information Table SI1).

3.1. Adsorption Kinetics and Thermodynamics in Powders

Prior to the adsorption studies, the crystal size distribution of CP and HP was determined by measuring the surface area of 1000 crystals per sample (**Figure 2**). Both materials could be represented by a Gaussian distribution with an average crystal radius of 36 nm and a standard deviation of 11.5 nm, confirming that the alkaline treatment did not alter the crystal size. This was important to eliminate crystal size effects as a parameter contributing to variations in the diffusion properties of the two samples.

3.1.1. Conventional Zeolite

The adsorption isotherm of 2,2DMB on CP at 338 K is shown in **Figure 3**. The maximum sorption capacity (80 mg g^{-1}) is slightly higher than previously reported literature values for MFI zeolites (60 mg g^{-1}).[35–37] In addition, the presence of strong hysteresis suggested the occurrence of capillary condensation at a relatively low pressure (ca. >2 mbar). This is in agreement with the small crystal size of the zeolite. In order to avoid the condensation phenomenon, which has a strong influence on the diffusivity[32] all further measurements are performed at low pressure (0.1 mbar).

The adsorption enthalpy ($-\Delta H$) of 2,2DMB was assessed by studying the amount adsorbed at equilibrium with varying temperature (**Figure 4**) according to the Van't Hoff equation (Equation 12):

$$K' = K'_0 \exp\left(-\frac{\Delta H}{RT}\right) \quad (12)$$

where K' is the Henry's constant, K'_0 the pre-exponential factor. The heat of adsorption derived over CP (27 kJ mol^{-1}, **Table 2**) is significantly lower than that previously reported (ca. 60 kJ mol^{-1}).[38–40] This difference is expected to originate from the small crystal size, and so high surface-to-volume ratio, of the zeolite studied, as a more pronounced contribution of the external surface could result in a decreased adsorption enthalpy.

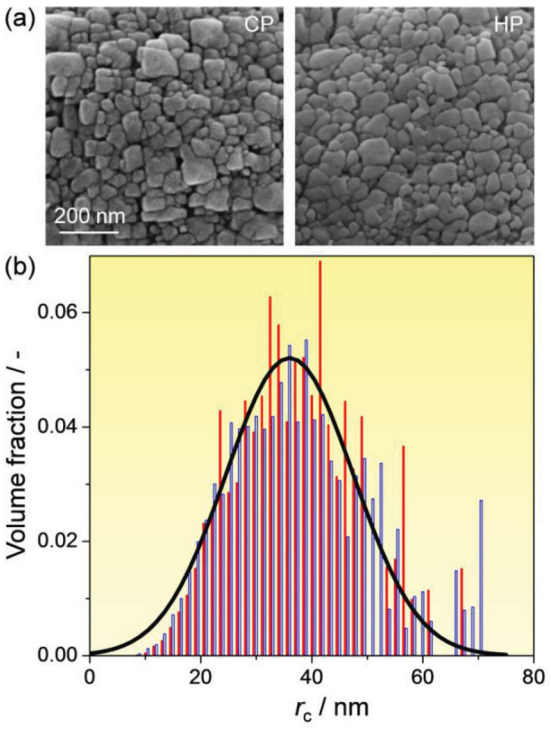

Figure 2. a) SEM images and b) crystal radius distribution of conventional (blue bars) and hierarchical (red bars) ZSM-5 powders. The fitted line represents a Gaussian distribution resulting in an average crystal radius of 36 nm with a standard deviation of 11.5 nm.

In order to assess the diffusion properties, i.e., the intracrystalline diffusivity and the activation energy, the transient uptake curves were measured at varying temperatures. The effective diffusivity of CP is shown in **Figure 5** together with previously

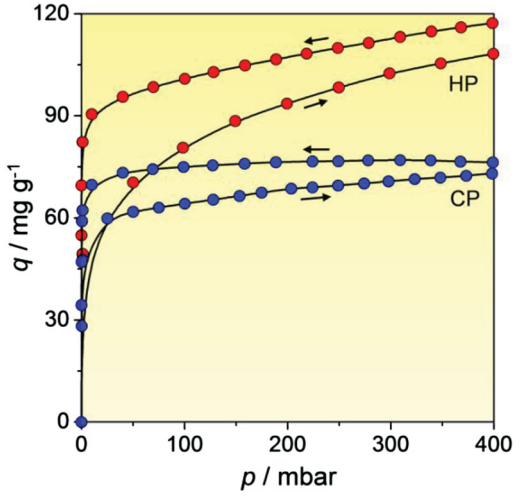

Figure 3. Adsorption isotherms of 2,2DMB on conventional and hierarchical ZSM-5 powders at 338 K.

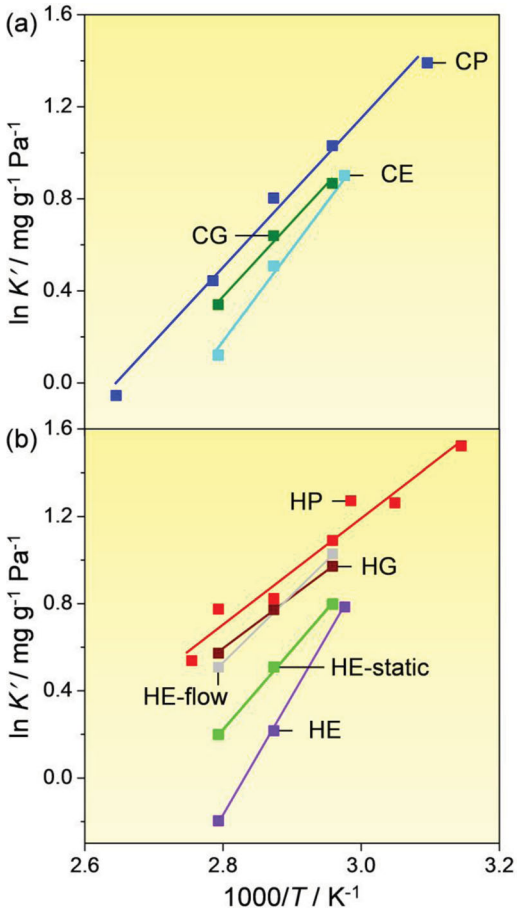

Figure 4. Arrhenius plot of the Henry's constant (K') of a) conventional and b) hierarchical ZSM-5 powders and their respective granules and extrudates.

Table 2. Heat of adsorption, $-\Delta H$, and activation energy, E_a, of 2,2DMB for the ZSM-5 samples studied in comparison with values reported in the literature.

Sample or Reference	$-\Delta H$ [kJ mol^{-1}]	E_a [a)] [kJ mol^{-1}]
CP	26.9	59.8
HP	20.1	52.3
CG	26.5	24.0
HG	20.1	21.1
CE	35.3	39.9
HE	44.7	35.1
HE-static	30.1	31.0
HE-flow	26	31.0
Silicalite-1[38]	55	68
Silicalite-1[40,41]	54.4	72.8[b)]
ZSM-5[39]	63.9	–
ZSM-5[3]	–	66.1
ZSM-5[37]	–	69.8

[a)]Derived from the effective diffusivity; [b)]Derived from the corrected diffusivity.

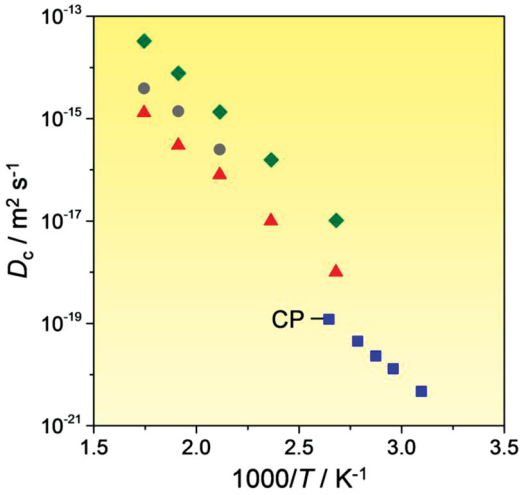

Figure 5. Effective diffusion coefficient (D_c) of conventional ZSM-5 powder (squares) as a function of temperature. Previously reported data are shown for comparison: Post et al.:[3] triangles; Xiao et al.:[37] diamonds; Jolimaitre et al.:[38] circles.

reported data on MFI-type samples.[3,37–38] Effective diffusivity instead of corrected diffusivity is chosen for comparison since no increase in the intracrystalline diffusion coefficient, D_c, was observed with the loading according to the Darken equation.[42] Indeed, a slight decrease of the diffusivity at very low loadings is noticed followed further by an independent behavior on the adsorbate concentration (vide infra). A similar pressure dependence has been reported for bulky alkanes.[3,37] The effective diffusivities obtained for CP are lower in comparison with literature values. Nevertheless, mass transfer is known to decrease on reduction of crystal size due to less controlled growth leading to internal defects or surface blockages.[34,41,43–45] The reduced mass transfer can also be attributed to the less than perfect nature of the commercially available zeolite crystals under investigation, in comparison with those more typically applied for kinetic measurements. The calculated activation energy of adsorption (E_a) showed a good agreement with reported values (Table 2).[3,37,41]

It is well known that resistance at the external surface could have a strong influence on the overall mass transfer, especially when small crystals are considered.[45–54] In order to investigate the presence and the contribution of surface barrier in the conventional zeolite, surface HF-etching treatments based on the methodology developed by Wloch et al.[51] have been applied. Accordingly, the template-containing zeolite and short HF exposures (5, 10, and 20 min) were used to avoid damaging the framework. The micropore volume and the amount of 2,2DMB adsorbed remained unaffected by the treatments (**Table 3**). XRD patterns of the etched samples confirmed the preserved crystallinity of the treated samples, while no impact on the crystal size and the morphology was observed by SEM imaging. The normalized uptake curves of the conventional samples treated for 5 and 20 min (CP-HF5 and CP-HF20) in **Figure 6** verified the effect of the treatment. The mass transfer is faster in the etched materials compared to the conventional zeolite. Furthermore, the normalized uptake curves of the

Table 3. Micropore volume, V_{micro}, and adsorbed amount of 2,2DMB, q, at 338 K and 0.1 mbar on the conventional ZSM-5 zeolite powder before and after HF treatment.

Sample code	Treatment time [min]	V_{micro} [$cm^3\ g^{-1}$]	q [$mg\ g^{-1}$]
CP	0	0.15	28.0
CP-HF5	5	0.15	31.9
CP-HF10	10	0.15	30.5
CP-HF20	20	0.15	32.4

samples treated for different times were very close indicating that the surface resistance was fully removed or at least strongly reduced after 5 min of the treatment and that the treatment for 20 min did not negatively impacted the crystallinity of the material. Nevertheless it is impossible to verify experimentally if the surface barrier is fully removed.

To quantify the eventual contribution of the surface barrier, the characteristic diffusion times related to the microporosity and surface resistance were compared assuming a linearly additive definition:[54]

$$t_{diff} = \frac{r_c^2}{D_{app}} = \frac{r_c^2}{D_c} + \frac{r_c}{3k_s} \quad (13)$$

where D_{app} and D_c are the apparent and intracrystalline diffusion coefficients, respectively, and k_s is the surface permeability. Since D_{app} is calculated using the uptake curve of the conventional zeolite and D_c is obtained from the uptake curve of the HF-etched sample, it is feasible to evaluate the surface resistance. The contribution of this barrier represents around 40% of the overall resistance and $k_s = 3 \times 10^{-13}$ m s^{-1}. The latter value correlates well with the literature.[54]

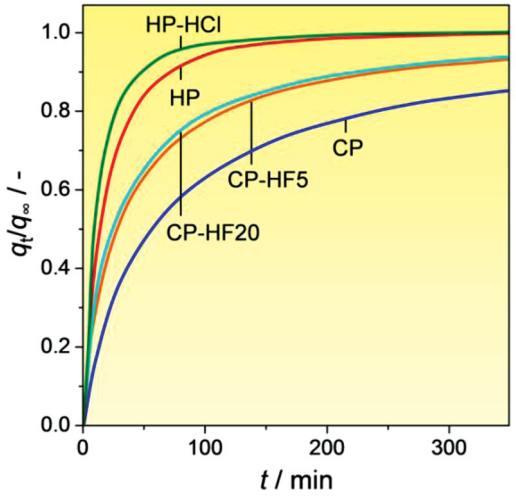

Figure 6. Normalized uptake curves of conventional and hierarchical ZSM-5 powders before and after treatments with HF or HCl.

3.1.2. Hierarchical Zeolites

In the pressure range studied, the adsorption isotherm of 2,2DMB on the hierarchical zeolite powder also exhibits a Langmuir-type behavior and pronounced hysteresis. The higher maximum adsorption capacity of HP compared to CP (120 mg g^{-1} and 80 mg g^{-1}, respectively) is indicative that capillary condensation not only occurs in the interspace between the crystals but also within the intracrystalline mesopores of the hierarchical zeolite. This observation demonstrates the accessibility of the mesopores introduced by desilication from the crystal surface.[55] A slightly lower enthalpy and activation energy of adsorption was evidenced for HP than CP (Table 2), the former confirming the assumption that an increase in surface area may lead to a decreased heat of adsorption.

Upon mesoporosity introduction, the normalized uptake curves (Figure 6) evidence a significantly improved mass transfer. The effective diffusivities derived for HP and CP were 6×10^{-20} and 1.3×10^{-20} $m^2\ s^{-1}$, respectively at 336 K and 0.1 mbar, revealing a 4.6 times enhancement for the hierarchical with respect to the conventional zeolite powder. This gain is of similar magnitude to other reported estimates (Table 1). Previously, it was suggested that imperfections resulting from alkali-induced leaching may cause resistance to diffusion at the crystal surface and/or at the interconnections of the micro- and mesopores within the zeolite.[20] To evaluate this hypothesis, we subjected the mesoporous zeolite to a sequential mild treatment with HCl, which is known to preferentially remove the realuminated species formed during desilication.[56] The acid washing enhanced the adsorption rate (sample HP-HCl, Figure 6), increasing the diffusivity by a factor of 1.3 compared to the alkaline-treated zeolite and 6 compared to the conventional zeolite. Similar improvement was observed on surface etching with HF (0.3 M HF, 5 min). These results clearly confirm that such a barrier to the mass transfer exists in the alkaline-treated zeolites, but that its relative impact is negligible and can be effectively reduced through the application of an appropriate treatment.

3.1.3. Mesopore Connectivity

If the improved mass transfer observed with the hierarchical sample resulted only from a shorter diffusion path in the presence of intracrystalline mesopores, a similar evolution of the effective diffusivity with the pore occupancy would be expected for both the hierarchical and conventional zeolites. However, comparison of the variation in effective diffusivity with 2,2DMB loading over CP and HP shows that this is clearly not the case (**Figure 7**). As mentioned, a slight decrease in D_c is observed at low loading for the conventional zeolite followed by a constant sorption rate. In contrast, the diffusivity in the hierarchical zeolite increases continuously with the loading, reaching a plateau at ca. 50 mg g^{-1}, corresponding to a pressure of 2–5 mbar, which arises due to capillary condensation. This behavior proves that the mesopores do not only shorten the diffusion pathway, but also contribute to the overall mass transfer process.[21,26–28,55,57]

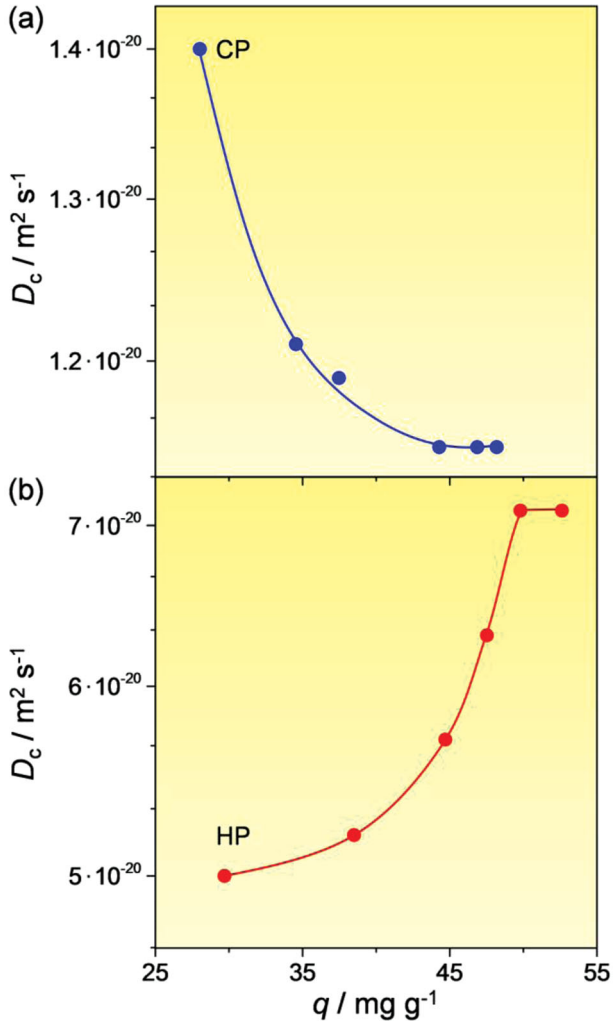

Figure 7. Effective intracrystalline diffusivity as a function of sample loading for a) conventional and b) hierarchical ZSM-5 powders.

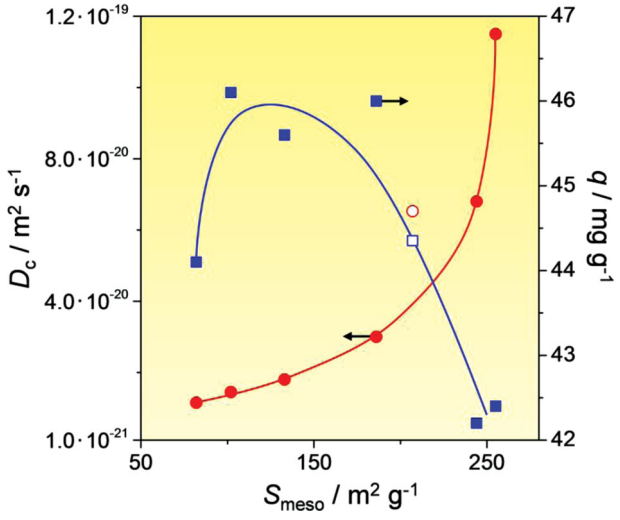

Figure 8. Effect of the mesopore surface area on a) the effective intracrystalline diffusivity (solid circles) and b) the adsorbed amount at the equilibrium (solid squares) for ZSM-5 powders prepared with varying time of alkaline treatment. Open symbols represent HP.

In order to assess the interdependence with the mesopore surface area (S_{meso}), the effective diffusivity was measured in hierarchical zeolites with distinct mesoporosity (**Figure 8**). To increase the population within the mesopores while avoiding capillary condensation, the measurements were performed at 0.5 mbar and 338 K. A linear relation between mesopore surface area and effective intracrystalline diffusivity was observed for samples of $S_{meso} < 150$ m^2 g^{-1}. This behavior is characteristic of mesopores acting as a shortcut to the micropores, leading to an enhancement of the diffusivity by a factor of ≈2. Above 150 m^2 g^{-1}, however, the intracrystalline diffusivity increases exponentially with increasing S_{meso}, indicating a greater involvement in the mass transfer. The parallel action of micro- and mesopores in the overall mass transfer led to an improvement of one order of magnitude under the experimental conditions used. The adsorption capacity of the samples is also reported in Figure 8. In the range corresponding to the linear evolution of the diffusivity with the mesopore surface, an increase of the adsorbed amount at the equilibrium is observed. Even if the origin of this enhancement is not clearly established, it could result from the impeded access of the hydrocarbon to some of the micropore volume due to the presence of surface or internal defects in CP. Then a decrease of the sorption capacity is seen, corresponding to the range of the exponential evolution of the diffusivity. This is due to the decreased of micropore volume occurring with the evolution of the mesoporous network. For comparative purposes, sample HP is shown in Figure 8 (open symbols) confirming the interconnected character of the mesoporous network established previously.

3.2. Adsorption Kinetics and Thermodynamics in Technical Bodies

Having rationalized the impact of mesopores on the intracrystalline diffusion in the zeolite powders, we were then able to verify the impact of shaping on the superior mass transfer properties observed for the desilicated ZSM-5.

3.2.1. Conventional Bodies

To confirm whether the introduction of binders and processing during shaping altered the thermodynamics of adsorption on the conventional zeolite, we first assessed the heat of adsorption for the shaped bodies. The conventional granules (CG) were found to exhibit an equivalent adsorption enthalpy (26.5 kJ mol^{-1}) as CP, while for the conventional extrudates (CE), a slight increase was observed (35.3 kJ mol^{-1}, Table 2). The thermodynamics of adsorption not only represent the affinity between the zeolite and the probe molecule, which can be altered by compositional/structural changes, but also governs the intra- (micropores) and extracrystalline (macropores) diffusivity (vide infra).[40]

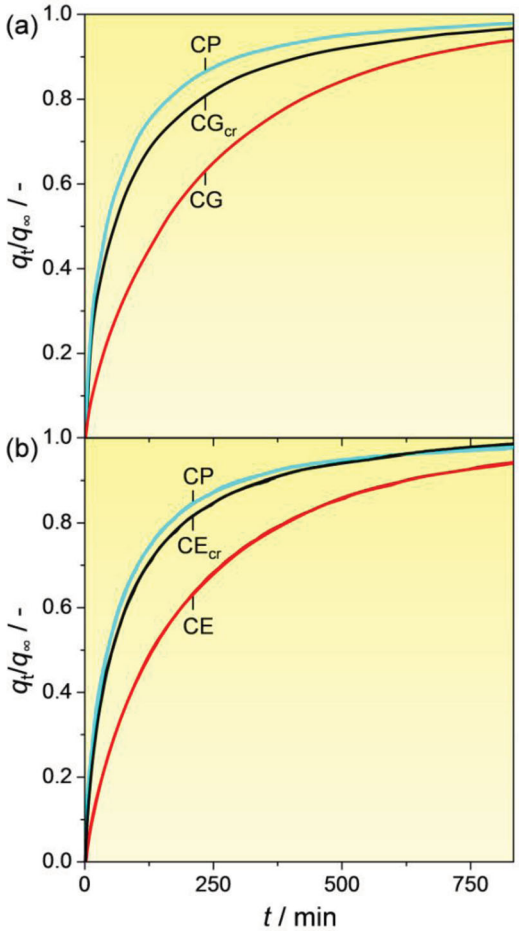

Figure 9. Effect of a) granulation and b) extrusion on the adsorption kinetics of conventional ZSM-5. CG_{cr} and CE_{cr} represent crushed granules and extrudates.

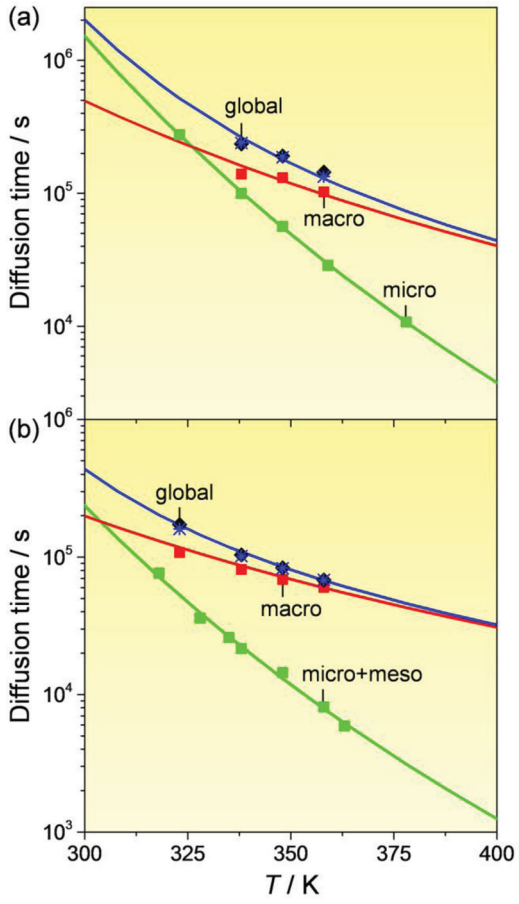

Figure 10. Contribution of the intra- (micro- or micro-/mesoporosity) and extracrystalline (macroporosity) resistances to the overall mass transfer for a) conventional and b) hierarchical granules as a function of temperature. The lines represent the theoretical evolution of resistances. The sum of the diffusion time in the intra- and extracrystalline porosity is also indicated (asterisks).

Notably slower uptake rates were observed for CG and CE with respect to their crushed (CG_{cr} and CE_{cr}) and pure powder (CP) analogues, consistent with a reduced mass transfer due to the influence of the additional macroporosity present in the granules (**Figure 9**a) and extrudates (Figure 9b). Since the kinetic measurements were performed at low pressure, the Knudsen regime can be considered as the controlling step in the macropores, while molecular and surface diffusions can be neglected. Assuming cylindrical macropores of radius 100 and 140 nm (in the absence of tortuosity), Knudsen diffusion coefficients of 1.9×10^{-5} and 2.7×10^{-5} m^2 s^{-1} are estimated for CG and CE, respectively at 338 K.

Figure 10a shows the experimental and calculated contributions of the intra- (microporosity) and extracrystalline (macroporosity) characteristic diffusion time constants to the overall mass transfer for CG. The close agreement between the global and total diffusion times unambiguously confirmed the validity of the determined diffusivity. This concurrence is obtained using tortuosity of 5.5 and 2.8 for CG and CE, respectively, and the estimated values are in a good agreement with commonly reported literature values.[1] The latter shows that the shaping process does not in this case influence the intracrystalline diffusivity or the surface barrier, e.g., by blocking pore mouths. It should be stressed that the contribution of the macroporosity to the overall mass transfer cannot be neglected in the wide temperature range investigated.

3.2.2. Hierarchical Bodies

In agreement with the observation for the powders, faster uptake rates were also observed for the hierarchical granules (HG) and hierarchical extrudates (HE) with respect to those of their conventional equivalents (**Figure 11**). This evidences the predominant retention of their beneficial function when the zeolite is shaped into technical form. The difference in the rate of uptake between the mesoporous shaped bodies and their crushed counterparts, affirms the significant contribution of the macroporosity to the overall mass transfer, similar to the case of the conventional bodies.

When the experimentally obtained uptake curves for the hierarchical zeolite bodies were fitted following the approach described for the conventional bodies, tortuosities of 5.5 and

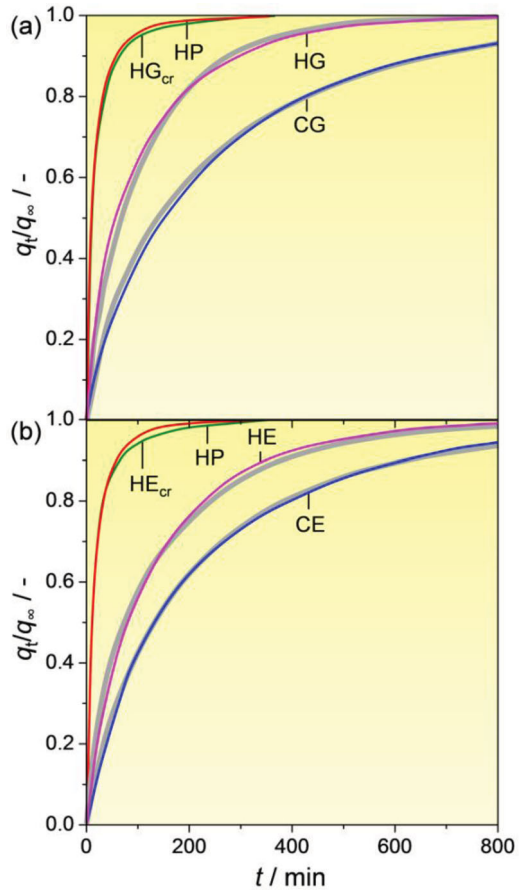

Figure 11. Comparison of the mass transfer in the conventional and hierarchical a) granules and b) extrudates. Grey lines represent the fits of the normalized uptake curves using Equations 2–5. HG_{cr} and HE_{cr} are the crushed hierarchical granules and extrudates.

3.8 were obtained for HG (r_{pore} = 140 nm) and HE (r_{pore} = 110 nm), respectively. These values correlate well with the tortuosities calculated for CG and CE indicating that the shaping process does not impair the enhanced diffusion in the hierarchical material by, for example, blocking the mesopores. Comparison of the intra- (micro/mesopores) and extracrystalline (macropores) resistances to the overall mass transfer (Figure 10b) exposes the dominating effect of macroporosity on the diffusion of 2,2DMB in the hierarchical granules. At 338 K the diffusion time within the intracrystalline micro-/mesopores represents only 20% of the overall mass transfer (instead of 40% for the conventional counterpart) and the contribution decreases rapidly with increasing temperature. In fact, the apparent activation energy of the global diffusion in HG (21 kJ mol^{-1}) is very close to the heat of adsorption (20 kJ mol^{-1}), confirming that the diffusion process is governed by the macroporosity. Interestingly, differences between the thermodynamics of adsorption were seen for the granules and the extrudates. In particular, a noticeably higher heat of adsorption was observed following extrusion of the zeolite powders with a kaolin binder which was most noticeable for the hierarchical zeolite (44.7 and 20.1 kJ mol^{-1} for HE and HP, respectively). No similar effect was observed upon granulation with the attapulgite binder. The modification of the adsorption enthalpy is important, since it reflects a change in the amount adsorbed at the equilibrium which in turn influences the effective intracrystalline diffusivity. Furthermore, the internal energy of adsorption also corresponds to the apparent activation energy of the mass transfer within the macropores. The similarity between the uptake curves of the hierarchical powder and the crushed hierarchical extrudates can be explained by the experimental conditions used (336 K and 0.1 mbar), under which the diffusivity is almost independent of the pressure. However, greater difference in the uptake rate can be expected when the loading is increased.

To gain further insight into the increased adsorption enthalpy observed, a second batch of hierarchical zeolite extrudates (2 mm diameter) of the same composition was prepared in at lab scale using a similar experimental procedure. The new hierarchical extrudates (HE-static) also exhibited a higher adsorption enthalpy than that of the powder (Figure 4), but lower than that of pilot-scale prepared HE (4 mm diameter). The difference in the heat of adsorption could arise due to the interaction of the zeolite with the binder, or as a result of the processing conditions. Since the variation in $-\Delta H$ was not observed over extrudates of the pure hierarchical zeolite, the former explanation is thought to be the most likely origin of this effect. To gain further insight, another batch of binder-containing hierarchical extrudates was prepared, but in this case the extrudates were calcined under an air flow (HE-flow). Measurement of the adsorption properties revealed that the adsorption enthalpy of the extrudates remained very close to those of HP. This indicates that the zeolite-binder interactions induced during sintering can be minimized by controlling the conditions of calcination. The understanding of such modifications is obviously of prime importance for the design of catalysts and adsorption techniques could provide a suitable tool to perform this investigation. However, a detailed study of the effects of zeolite-binder interactions is beyond the scope of the present manuscript, devoted to the origins of mass transfer improvements in hierarchical zeolite bodies, and will be addressed in detail in future work.

4. Conclusions

By validation of a suitable methodology, this work demonstrated that the enhanced properties of hierarchical zeolite powders were fully retained when shaped into millimeter-sized technical forms. Gravimetric experiments evidenced over 5 times faster diffusion of 2,2-dimethylbutane in the hierarchical zeolite vis-à-vis its conventional counterpart. The origin of the improved performance was directly linked to the presence of the interconnected networks of micro- and mesopores within the zeolite crystals. These effects were not explicable purely due to a possible reduction in the crystal size or in the surface barrier due to the modifications induced by alkali leaching. Furthermore, the direct participation of mesopores in the kinetics and thermodynamics of adsorption indicated that their role in facilitating molecular diffusion is more substantial that simply shortening the diffusion path in the micropores. The molecular transport

in agglomerated systems was governed by the diffusion in the macropores, which represented between 50–80% of the overall mass transfer at 338 K and 0.1 mbar, and increased rapidly with temperature. Adsorption measurements proved an efficient tool to assess the impact of the shaping process and of binder-active phase interactions. For the hierarchical zeolites studied, the mechanical forces exerted during granulation or extrusion had no noticeably impact on the derived kinetics and thermodynamic parameters. In contrast the adsorption properties were altered by the type of binder and calcination conditions applied. The latter is of great potential interest to detect and understand compositional and structural changes occurring during catalyst scale-up. Quantification of mass transfer resistances in hierarchical bodies is of practical relevance to design more efficient catalytic processes. Our results indicate that no significant gain in the total time needed for a molecule to diffuse through the entire zeolite extrudate or granule is expected. Nevertheless, the Thiele modulus and the effectiveness factor, which describe the utilization of the zeolite crystal, can be drastically improved. The concentration gradient through the zeolite crystals will be considerably lower, improving the catalytic performance of the mass transfer-limited reactions which explains the largely improved performances in the conversion of methanol to olefins reported previously.[31]

5. Experimental Section

Zeolite Preparation and Shaping: A ZSM-5 zeolite with a nominal molar Si/Al ratio of 40 prepared at Zeochem's production site (Uetikon, Switzerland),[29] was used as a starting material. The conventional zeolite powder (CP) was obtained by calcination in flowing dry air at 753 K for 3 h. Its hierarchical form (HP) was prepared by treatment in aqueous NaOH (0.2 M, 30 L per kg of zeolite) at 338 K for 30 min, using a mechanically stirred 50 L reactor. To obtain zeolites with different extent of mesoporosity, the conventional zeolite powder was subjected to alkaline treatment with varying time from 5 to 25 min (HP-*x* where *x* represents the treatment time) in stirred aqueous NaOH solution (0.2 M, 30 cm^3 per gram of zeolite) at 338 K using an Easymax 102 reactor system from Mettler Toledo. The resulting suspensions were quenched in an ice-water mixture, and the alkaline-treated samples were collected by filtration, washed and dried. All zeolites were converted into the ammonium form by three consecutive treatments with aqueous NH_4NO_3 (0.1 M, 6 h). The isolated solids were washed extensively with distilled water, dried at 338 K and calcined as described for CP.

Etching with HF (1.35 M) to remove surface imperfections was performed on the as-synthesized zeolite powder containing the TPA^+ template. The zeolite (3 g) and acetone (30 cm^3) were introduced into a Teflon container. Following addition of HF (1.62 g, 50 wt% in water), the mixture was stirred at room temperature for 5, 10, or 20 min, filtered, and extensively washed with acetone and distilled water. The collected solids were dried at 423 K for 2 h and calcined in an air flow at 823 K for 10 h (5 K min^{-1}). A similar etching procedure was applied to the protonic form of the hierarchical zeolite (i.e., in the absence of organic template) which was treated for 5 min with the HF solution (0.3 M). Mild acid washing of the desilicated zeolite powder was conducted in aqueous HCl solution (0.05 M, 100 cm^3 per g of zeolite) at 338 K for 6 h.

As detailed elsewhere,[31] conventional and hierarchical zeolite powders in protonic form were structured into mechanically stable granules (2–3 mm diameter) by pan granulation with high-purity attapulgite (20 wt%) or into extrudates (4 mm diameter) by extrusion with kaolin (20 wt%). The resulting granules (CG and HG) or extrudates (CE and HE) were dried and calcined for 5 h at 823 K in flowing dry air or 873 K under static conditions using 5 K min^{-1}, respectively. Additionally, 2 mm diameter extrudates of hierarchical zeolite with and without binder addition were prepared in a single Mini Screw Extruder (Caleva). The physical mixtures for the extrusion were homogenized using a Mixer Torque Rheometer 3 (Caleva). Binderless extrudates were calcined in static air, while extrudates shaped with kaolin were calcined in static air (HE-static) and in an air flow (HE-flow) at 873 K with a heating ramp of 5 K min^{-1}.

Characterization and Adsorption Measurements: N_2 isotherms at 77 K were measured in a Quantachrome Quadrasorb-SI analyzer after evacuation of the samples at 573 K for 10 h. The zeolite crystal size distribution was determined by SEM imaging using a Zeiss Gemini 1530 FEG microscope. The adsorption of 2,2DMB (>99%, ABCR) was performed in an Intelligent Gravimetric Analyzer (IGA-002, Hiden Isochema). Prior to analysis, the size selection of powders and shaped samples (25–30 mg) were outgassed in situ at 573 K for 4 h under vacuum (10^{-5} bar). When a desired temperature of an experiment was stabilized, the sample was subjected to a pressure step of 2,2DMB vapor and the weight change was continuously recorded until equilibrium was reached.

Supporting Information

Supporting Information is available from the Wiley Online Library or from the author.

Acknowledgements

The Swiss National Science Foundation (project number 200021-134572) is acknowledged for financial support. N.-L. Michels is thanked for assistance with sample preparation and characterization.

Received: December 2, 2012
Revised: January 12, 2013
Published online: April 4, 2013

[1] J. Kärger, D. M. Ruthven, *Diffusion in Zeolites and Other Microporous Solids*; John Wiley & Sons, New York **1992.**
[2] J. Kärger, D. Freude, *Chem. Eng. Technol.* **2002**, *25*, 769.
[3] M. F. M. Post, J. van Amstel, H. W. Kouwenhoven, in Proc. 6th Int. Zeolite Conf., *Reno, NV, USA, 1983*; (Ed: D. Olson, A. Bisio), Butterworths, Guildford, Surrey, UK **1984**; p. 517–527.
[4] A. Corma, M. J. Díaz-Cabañas, J. Martínez-Triguero, F. Rey, J. Rius, *Nature* **2002**, *418*, 514.
[5] A. Corma, M. J. Díaz-Cabañas, F. Rey, S. Nicolopoulus, K. Boulahya, *Chem. Commun.* **2004**, 1356.
[6] C. C. Freyhardt, M. Tsapatsis, R. F. Lobo, K. J. Balkus Jr., M. E. Davis, *Nature* **1996**, *381*, 295.
[7] J. Pérez-Ramírez, C. H. Christensen, K. Egeblad, C. H. Christensen, J. C. Groen, *Chem. Soc. Rev.* **2008**, *37*, 2530.
[8] J. Pérez-Ramírez, *Nat. Chem.* **2012**, *4*, 250.
[9] S. van Donk, A. H. Janssen, J. H. Bitter, K. P. de Jong, *Catal. Rev.* **2003**, *45*, 297.
[10] A. Corma, V. Fornes, S. B. Pergher, Th. L. M. Maesen, J. G. Buglass, *Nature* **1998**, *396*, 353.
[11] W. J. Roth, J. Čejka, *Catal. Sci. Technol.* **2011**, *1*, 43.
[12] D. Verboekend, J. Pérez-Ramírez, *Catal. Sci. Technol.* **2011**, *1*, 879.
[13] M. S. Holm, E. Taarning, K. Egeblad, C. H. Christensen, *Catal. Today* **2011**, *168*, 3.
[14] J. C. Groen, W. Zhu, S. Brouwer, S. J. Huynink, F. Kapteijn, J. A. Moulijn, J. Pérez-Ramírez, *J. Am. Chem. Soc.* **2007**, *129*, 355.
[15] L. Zhao, B. Shen, J. Gao, C. Xu, *J. Catal.* **2008**, *258*, 228.

[16] D. Tzoulaki, A. Jentys, J. Pérez-Ramírez, K. Egeblad, J. A. Lercher, *Catal. Today* **2012**, *198*, 3.
[17] C. H. Christensen, K. Johannsen, E. Törnqvist, I. Schmidt, H. Topsøe, C. H. Christensen, *Catal. Today* **2007**, *128*, 117.
[18] F. C. Meunier, D. Verboekend, J.-P. Gilson, J. C. Groen, J. Pérez-Ramírez, *Microporous Mesoporous Mater.* **2012**, *148*, 115.
[19] D. Mehlhorn, R. Valiullin, J. Kärger, K. Cho, R. Ryoo, *ChemPhysChem* **2012**, *13*, 1495.
[20] D. Mehlhorn, R. Valiullin, J. Kärger, K. Cho, R. Ryoo, *Materials* **2012**, *5*, 699.
[21] P. Kortunov, S. Vasenkov, J. Kärger, R. Valiullin, P. Gottschalk, M. Fé Elía, M. Perez, M. Stöcker, B. Drescher, G. McElhiney, C. Berger, R. Gläser, J. Weitkamp, *J. Am. Chem. Soc.* **2005**, *127*, 13055.
[22] H. Vinh-Thang, Q. Huang, A. Ungureanu, M. Eić, D. Trong-On, S. Kaliaguine, *Langmuir* **2006**, *22*, 4777.
[23] R. Valiullin, J. Kärger, K. Cho, M. Choi, R. Ryoo, *Microporous Mesoporous Mater.* **2011**, *142*, 236.
[24] D. Verboekend, J. C. Groen, J. Pérez-Ramírez, *Adv. Funct. Mater.* **2010**, *20*, 1441.
[25] D. Verboekend, R. Caicedo-Realpe, A. Bonilla, M. Santiago, J. Pérez-Ramírez, *Chem. Mater.* **2010**, *22*, 4679.
[26] P. Zeigermann, S. Naumov, S. Mascotto, J. Kärger, B. M. Smarsly, R. Valiullin, *Langmuir* **2012**, *28*, 3621.
[27] F. Furtado, P. Galvosas, M. Gonçalves, F.-D. Kopinke, S. Naumov, F. Rodríguez-Reinoso, U. Roland, R. Valiullin, J. Kärger, *J. Am. Chem. Soc.* **2011**, *133*, 2437.
[28] R. Valiullin, J. Kärger, *Chem. Ing. Tech.* **2011**, *83*, 166.
[29] J. Pérez-Ramírez, S. Mitchell, D. Verboekend, M. Milina, N.-L. Michels, F. Krumeich, N. Marti, M. Erdmann, *ChemCatChem* **2011**, *3*, 1731.
[30] N.-L. Michels, S. Mitchell, M. Milina, K. Kunze, F. Krumeich, F. Marone, M. Erdmann, N. Marti, J. Pérez-Ramírez, *Adv. Funct. Mater.* **2012**, *22*, 2509.
[31] S. Mitchell, N.-L. Michels, K. Kunze, J. Pérez-Ramírez, *Nat. Chem.* **2012**, *4*, 825.
[32] J. Kärger, D. M. Ruthven, D. N. Theodorou, *Diffusion in Nanoporous Materials*, Wiley-VCH Verlag GmbH, Weinheim **2012**.
[33] D. M. Ruthven, K. F. Loughlin, *Chem. Eng. Sci.* **1971**, *26*, 577.
[34] D. M. Ruthven, *Principles of adsorption and adsorption processes*, John Wiley & Sons, New York **1984**.
[35] R. Krishna, *Chem. Eng. Res. Des.* **2001**, *79*, 182.
[36] S. Calero, B. Smit, R. Krishna, *Phys. Chem. Chem. Phys.* **2001**, *3*, 4390.
[37] J. Xiao, J. Wei, *Chem. Eng. Sci.* **1992**, *47*, 1123.
[38] E. Jolimaitre, M. Tayakout-Fayolle, C. Jallut, K. Ragil, *Ind. Eng. Chem. Res.* **2001**, *40*, 914.
[39] J. F. Denayer, W. Souverijns, P. A. Jacobs, J. A. Martens, G. V. Baron, *J. Phys. Chem. B* **1998**, *102*, 4588.
[40] C. L. Cavalcante Jr., D. M. Ruthven, *Ind. Eng. Chem. Res.* **1995**, *34*, 177.
[41] C. L. Cavalcante Jr., D. M. Ruthven, *Ind. Eng. Chem. Res.* **1995**, *34*, 185.
[42] D. R. Garg, D. M. Ruthven, *Chem. Eng. Sci.* **1972**, *27*, 417.
[43] J. Kärger, J. Caro, *J. Chem. Soc., Faraday Trans. 1* **1977**, *73*, 1363.
[44] S. J. Reitmeier, O. C. Gobin, A. Jentys, J. A. Lercher, *J. Phys. Chem. C* **2009**, *113*, 15355.
[45] M. Bülow, P. Struve, G. Finger, C. Redszus, K. Ehrhardt, W. Schirmer, J. Kärger, *J. Chem. Soc., Faraday Trans. 1* **1980**, *76*, 597.
[46] J. Kärger, W. Heink, H. Pfeifer, M. Rauscher, J. Hoffmann, *Zeolites* **1982**, *2*, 275.
[47] M. Krutyeva, S. Vasenkov, X. Yang, J. Caro, J. Kärger, *Microporous Mesoporous Mater.* **2007**, *104*, 89.
[48] A. Micke, M. Bülow, M. Kočiřík, *J. Phys. Chem.* **1994**, *98*, 924.
[49] D. Tzoulaki, L. Heinke, W. Schmidt, U. Wilczok, J. Kärger, *Angew. Chem. Int. Ed.* **2008**, *47*, 3954.
[50] D. Tzoulaki, W. Schmidt, U. Wilczok, J. Kärger, *Microporous Mesoporous Mater.* **2008**, *110*, 72.
[51] J. Wloch, *Microporous Mesoporous Mater.* **2003**, *62*, 81.
[52] L. Zhang, C. Chmelik, A. N. C. van Laak, J. Kärger, P. E. de Jongh, K. P. de Jong, *Chem. Commun.* **2009**, 6424.
[53] D. M. Ruthven, L. Heinke, J. Kärger, *Microporous Mesoporous Mater.* **2010**, *132*, 94.
[54] L. Gueudré, E. Jolimaître, N. Bats, W. Dong, *Adsorption* **2010**, *16*, 17.
[55] T. Kirchner, A. Shakhov, P. Zeigermann, R. Valiullin, J. Kärger, *Carbon* **2012**, *50*, 4804.
[56] D. Verboekend, S. Mitchell, M. Milina, J. C. Groen, J. Pérez-Ramírez, *J. Phys. Chem. C* **2011**, *115*, 14193.
[57] D. Mehlhorn, R. Valiullin, J. Kärger, K. Cho, R. Ryoo, *Microporous Mesoporous Mater.* **2012**, *164*, 273.